

## Coulomb scattering rates of excited carriers in moderate-gap carbon nanotubes

C. W. Chiu,<sup>1</sup> F. L. Shyu,<sup>2</sup> C. P. Chang,<sup>3</sup> D. S. Chuu,<sup>4</sup> and M. F. Lin<sup>1</sup><sup>1</sup>Department of Physics, National Cheng Kung University, Tainan, Taiwan<sup>2</sup>Department of Physics, Chinese Military Academy, Kaohsiung, Taiwan<sup>3</sup>Center for General Education, Tainan Woman's College of Art and Technology, Tainan, Taiwan<sup>4</sup>Department of Physics, National Chiao Tung University, Hsinchu, Taiwan

(Received 10 November 2005; revised manuscript received 26 April 2006; published 12 June 2006)

Temperature induces some free carriers in moderate-gap carbon nanotubes, which, thus, creates the low-frequency intraband  $e$ - $h$  excitations. Such excitations are the effective deexcitation channels for the excited electrons (holes) in conduction (valence) bands, while they are very weak. The Coulomb decay rates of the lowest two conduction bands are sensitive to the changes in wave vector, radius, and temperature. However, those of the band-edge states depend on chirality weakly. These results directly reflect the strong energy dispersions and the temperature-dependent electron distributions. The calculated results are roughly consistent with the experimental measurements from the ultrafast optical spectroscopies.

DOI: 10.1103/PhysRevB.73.235407

PACS number(s): 73.63.Fg, 71.10.-w, 71.45.Gm

Quasi-one-dimensional carbon nanotubes (CNs) have resulted in a lot of interesting properties.<sup>1–26</sup> Each single-walled cylindrical nanostructure is characterized by the  $(m, n)$  indices which specify radius and chirality.<sup>4</sup> Measurements of scanning tunneling microscopy<sup>5,6</sup> show that CNs are moderate-gap semiconductors for  $2m+n \neq 3I$  ( $I$  an integer), metals for  $m=n$ , and narrow-gap semiconductors for others. The rich energy spectra would be directly reflected in electronic excitations and deexcitations. When electrons are excited from occupied states to unoccupied states by the Coulomb or electromagnetic field, they could further decay by the inelastic  $e$ - $e$  scatterings. In this work, we mainly study the Coulomb scattering rates of the excited carriers in the lowest two conduction bands of moderate-gap CNs. The dependence of the inverse lifetime ( $1/\tau$ ) on excitation channels, temperature, wave vector, radius, and chirality is investigated.

The femtosecond pump-probe spectroscopies are powerful tools in researching the ultrafast relaxation of photoexcited electrons in moderate-gap CNs. Experimental measurements are made on bundled and isolated single-walled CNs by using the time-resolved absorption<sup>11–15</sup> and fluorescence spectroscopies.<sup>16–19</sup> The fast decay time of the first (second) conduction band is  $\tau \sim 0.3$ – $1.5$  ps (Refs. 11–15 and 18) ( $\tau \sim 0.13$ – $0.77$  ps),<sup>11–13,15</sup> which depends on nanotube geometry or energy gap.  $\tau$  is deduced to come from the intraband carrier deexcitations. These results suggest that the  $e$ - $e$  Coulomb interactions may play an important role on the carrier relaxation. The first conduction band also exhibits a slow decay time ( $\tau'$ ). The measured value has a wide range  $\tau' \sim 5$ – $30$  ps (Refs. 13 and 15–17) and  $\sim 120$  ps.<sup>14</sup>  $\tau'$  was attributed to the interband recombination or the defect trapping. The temperature-dependent photoluminescence (PL) spectra were made on the very small (6,4) CN between 48 K and 182 K.<sup>19</sup> The decay time of the first conduction band is about 100 ps–20 ps. The PL decay, which exhibits the monoexponential behavior, is deduced to be associated with the nonradiative decay of excitons. The third kind of femtosecond spectroscopy, the time-resolved photoelectron spectroscopy, has been used to study the carrier relaxation of

the excited electrons in metallic single-walled<sup>20</sup> and multiwalled<sup>21</sup> CNs. The measured lifetime is  $\tau \sim 0.2$  ps for the low energy excited states.

For metallic and moderate-gap CNs at  $T=0$ , the inverse electron lifetimes due to the Coulomb interactions were calculated by the self-energy in the previous study.<sup>10</sup> A simple relation between wave vector and decay rate is found to be absent. The lowest two conduction bands in moderate-gap CNs have the vanishing decay rates, mainly owing to the absence of the low-frequency deexcitation channels. The present study considers the effects of temperature on the decay rates in moderate-gap CNs. The decay rates of the excited carriers (electrons or holes) are evaluated from the generalized finite-temperature self-energy. This allows us to compare the calculated inverse lifetimes with those obtained from the experimental measurements.<sup>11–19</sup>

In general, the moderate-gap CNs have band gaps much higher than the thermal energy at room temperature. The free carrier density is very low, and so is the intensity of electronic excitations. The unique cylindrical symmetry makes CNs exhibit the decoupled excitation spectra of different angular momenta ( $L$ 's).<sup>7–9</sup> The intraband electron-hole ( $e$ - $h$ ) excitations of  $L=0$  have the lowest excitation frequencies. Whether such very weak excitations are the effective relaxation channels is worthy of a detailed investigation. The electronic excitations of  $L=0$  would be studied by evaluating the longitudinal dielectric function ( $\epsilon$ ) within the random-phase approximation (RPA).<sup>7</sup>  $\epsilon$  can provide a full understanding of the effective  $e$ - $e$  interactions during the inelastic Coulomb scatterings.

The  $(m, 0)$  zigzag CNs are chosen for a model study. The energy dispersion ( $E^{c,v}(k_y, J)$ ) is calculated from the nearest-neighbor tight-binding model.<sup>4</sup> Conduction bands are symmetric to valence bands about the Fermi level  $E_F=0$ . Each state is described by the axial wave vector  $|k_y| \leq \pi/3b$  and the angular momentum  $J=1, 2, \dots, 2m$ . Zigzag CNs, with  $m \neq 3I$  are moderate-gap semiconductors ( $E_g \approx 1.5\gamma_0 b/r$ ), as shown in Figs. 1(a)–1(d). At room temperature, there are some free electrons (holes) in the lowest conduction (valence) band nearest to  $E_F=0$ . These carriers would induce

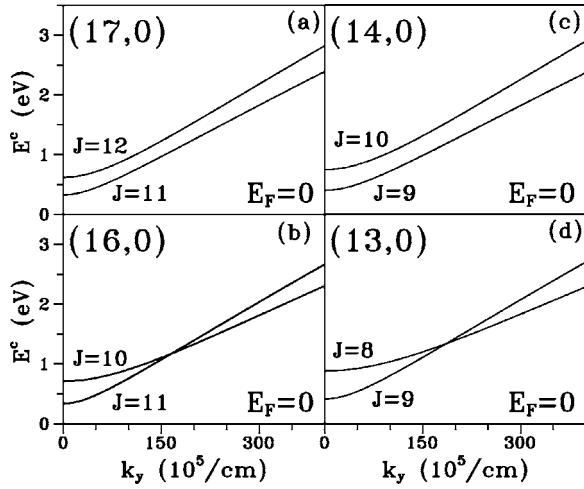


FIG. 1. The first two conduction bands for (a) (17,0), (b) (16,0), (c) (14,0), (d) (13,0) CNs.

the single-particle excitations and thus provide the deexcitation channels for the inelastic Coulomb scatterings. The dependence of energy on wave vector would determine the decay energies of the excited electrons. The ratio of the effective mass between the first and the second conduction bands are, respectively, 1.4, 3.2, 1.3; 3.4 for the (17,0), (16,0), (14,0); (13,0) CNs. The second conduction band has the weaker  $k_y$  dependence, especially for the (13,0) and (16,0) CNs.

The transferred momentum ( $q$ ) and angular momentum ( $L$ ) are conserved in the  $e$ - $e$  interactions. The low-frequency electronic excitations correspond to the  $L=0$  case. The temperature-dependent dielectric function of  $L=0$  is calculated within the RPA.<sup>7</sup> At  $T=0$ ,  $\epsilon(q, L=0, \omega)$  purely comes from the  $v \rightarrow c$  interband excitations (occupied valence states to unoccupied conduction states). Such  $e$ - $h$  excitations occur at the sufficiently high energy  $\omega \geq E_g$  so that they do not make any contribution to the low energy decay rate. However, the  $T$ -induced free carriers can create the low-frequency intraband excitations ( $c \rightarrow c$  and  $v \rightarrow v$ ). The imaginary part ( $\epsilon_2$ ) and the real part ( $\epsilon_1$ ) of the  $L=0$  dielectric function are, respectively, shown in Figs. 2(a) and 2(b) at  $T=300$  K and  $q=0.1$  ( $10^5/\text{cm}$  here and henceforth).  $\epsilon_2$ , which characterizes the  $e$ - $h$  excitations, exhibits a weak peak at excitation energy  $\omega_{ex}$ . The intraband excitations only survive at low  $\omega_{ex}$ . The peak height in  $\epsilon_2$  grows with increasing carrier density so that the large CNs have the stronger  $e$ - $h$  excitations. The corresponding  $\epsilon_1$  exhibits a shallow diplike structure near  $\omega_{ex}$ . As a result, there is a weak peak in the loss function at  $\omega_{ex}$  [ $\text{Im}(-1/\epsilon)$  in Fig. 2(c)]. The prominent peak is absent; that is, some free carriers do not cause collective excitations or plasmon. The low-frequency excitation spectrum is completely dominated by the intraband  $e$ - $h$  excitations. It is too weak to be observed in the electron-energy-loss spectroscopy. However, the loss function is very useful in understanding the Coulomb decay rates.

As to the lowest two conduction bands, the electronic excitations of  $L=0$  are responsible for the inelastic Coulomb scattering rates. The decay rate of the excited carrier in the  $(k_y, J, h)$  state is associated with the screened exchange energy<sup>10</sup>

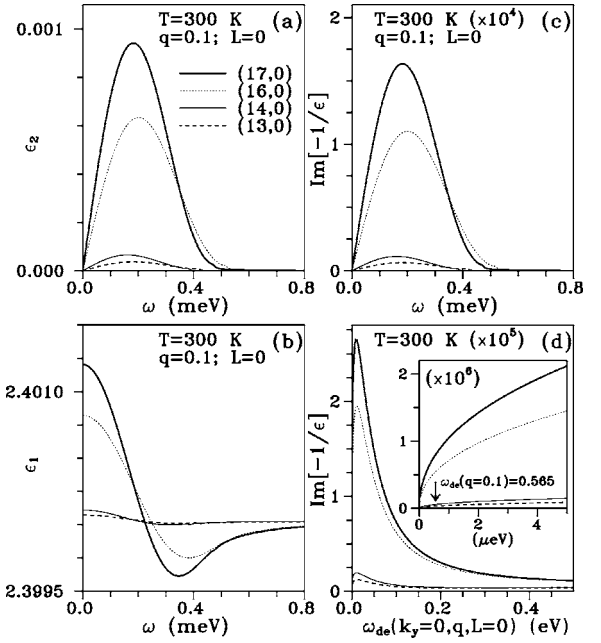


FIG. 2. The  $L=0$  intraband excitations of moderate-gap CNs at  $T=300$  K. (a) The imaginary part and (b) the real part of the dielectric function; (c) the loss spectrum are shown at  $q=0.1$ . (d) shows the loss spectrum associated with the  $k_y=0$  band-edge state in the first conduction band.

$$\Sigma(k_y, J, h, ik_n) = -\frac{1}{\beta} \sum_{q, h', m} V^{\text{eff}}(q, L=0, i\omega_m; k_y, J, h, h') G^{(0)} \times (k_y + q, J, h', ik_n + i\omega_m). \quad (1)$$

$V^{\text{eff}} = V(q, L=0) |\langle k_y + q, J, h' | e^{iqy} | k_y, J, h \rangle|^2 / \epsilon(q, L=0, i\omega_m)$  is the screened Coulomb interactions.<sup>7</sup>  $\beta = 1/k_B T$ ,  $k_n = (2n+1)\pi/\beta$ ,  $\omega_m = 2m\pi/\beta$ , and  $G^{(0)}$  is the noninteracting Matsubara Green's function. The analytic continuation  $ik_n \rightarrow E^h(k_y, J)$  is done, and the self-energy is divided into the line part and the residue part.  $\Sigma(k_y, J, h) = \Sigma^{(\text{line})}(k_y, J, h) + \Sigma^{(\text{res})}(k_y, J, h)$ , where the line part is similar to Eq. (1), but with  $ik_n$  replaced by  $E^h(k_y, J)$ . The real line-part self-energy is independent of the quasiparticle lifetime. The residue-part self-energy is

$$\begin{aligned} \Sigma^{(\text{res})}(k_y, J, h, ik_n \rightarrow E^h(k_y, J)) &= -\frac{1}{\beta} \sum_{q, h', m} V^{\text{eff}}(q, L=0, i\omega_m; k_y, J, h, h') \\ &= 0, i\omega_m; k_y, J, h, h') \\ &\times \left( \frac{1}{ik_n + i\omega_m - E^{h'}(k_y + q, J)} - \frac{1}{E^h(k_y, J) + i\omega_m - E^{h'}(k_y + q, J)} \right). \end{aligned} \quad (2)$$

By doing the frequency summation, the inverse carrier lifetime is characterized by

$$\begin{aligned}
& -2 \operatorname{Im} \Sigma^{(\text{res})}(k_y, J, h) \\
&= -2 \sum_{q, h'} \operatorname{Im}[-V^{\text{eff}}(q, L \\
&= 0, \omega_{de}; k_y, J, h, h')] \\
&\quad \times (n_B(-\omega_{de})\{1 - n_F[E^{h'}(k_y + q, J)]\} \\
&\quad - n_B(\omega_{de})\{n_F[E^{h'}(k_y + q, J)]\}) \\
&= \frac{1}{\tau_e(k_y, J, h)} + \frac{1}{\tau_h(k_y, J, h)}. \quad (3)
\end{aligned}$$

$n_F$  and  $n_B$  are the Fermi and Bose distribution functions, respectively. At finite temperature,  $-2 \operatorname{Im} \Sigma^{(\text{res})}$  consists of electron and hole decay rates. As a result of the band symmetry,  $1/\tau_e(k_y, J, c) = 1/\tau_h(k_y, J, v)$  and  $1/\tau_e(k_y, J, v) = 1/\tau_h(k_y, J, c)$ . The ratio between the former and the latter is about  $10^5$ , mainly owing to the serious restriction on the final-state distribution functions. The photon absorption could produce an electron in conduction band and a hole in valence band, so the total decay rate is  $1/\tau = 1/\tau_e(k_y, J, c) + 1/\tau_h(k_y, J, v) = 2/\tau_e(k_y, J, c)$ . This work is focused on decay rates of excited electrons in the lowest two conduction bands. The first term  $\operatorname{Im}[-V^{\text{eff}}(\omega_{de})]$  in Eq. (3) is proportional to the loss function, and the second term  $n_B(-\omega_{de})\{1 - n_F[E^{h'}(k_y + q, J)]\}$  is associated with the number of deexcitation channels. The  $(k_y, J, c)$  state could be deexcited to the  $(k_y + q, J, c)$  state (the intraband decay) or the  $(k_y + q, J, v)$  state (the interband decay). The final-state electron distributions make the interband decay negligible. In general, the intraband decay energy  $\omega_{de} = E^c(k_y, J) - E^c(k_y + q, J)$  [inset in Fig. 2(d)] is not equal to the excitation energy  $\omega_{ex}$ .  $\omega_{de}$  must be positive at  $T=0$ . Electronic deexcitations, with negative decay energies, are allowed at finite temperature, while they are limited by  $n_B(-\omega_{de})$ . The loss function in Eq. (3) is an odd function of  $\omega_{de}$ . Moreover,  $\operatorname{Im}[-1/\epsilon(\omega_{de})]$  is dominated by the small- $(q, \omega_{de})$  transfer, as shown in Fig. 2(d) for the  $k_y=0$  state in the first conduction band.

The Coulomb scattering rates of the first conduction band are shown in Fig. 3(a) at room temperature. There is no simple relation between decay rate and wave vector.  $1/\tau_e$  declines quickly as  $k_y$  gradually deviates from the band-edge state. The  $k_y=0$  state exhibits the strongest decay rate. This state is deexcited to higher states under the negative energy transfer, but not the positive energy transfer [inset in Fig. 3(a)]. For example,  $1/\tau_e(k_y=0, J=11, c)$  of the (17,0) CN is about 3.25 meV ( $\tau_e \sim 1.23$  ps). The decay rate of the band-edge state becomes faster in the increment of the nanotube radius. This result clearly illustrates that the increasing carrier density significantly enhances the intraband loss spectrum and thus the decay rate. As to other states, the decay rates under the negative energy transfer are comparable to those under the positive energy transfer.

The intraband decay rate of the band-edge state is mainly determined by  $\operatorname{Im}[-V^{\text{eff}}(\omega_{de})]$  and  $n_B(-\omega_{de})\{1 - n_F[E^c(k_y + q, J)]\}$  [Eq. (3)].  $1 - n_F[E^c(k_y + q, J)]$  is about 1 for the intraband decay, and the second term only depends on  $n_B(-\omega_{de})$ . The effective deexcitation channels occur at very

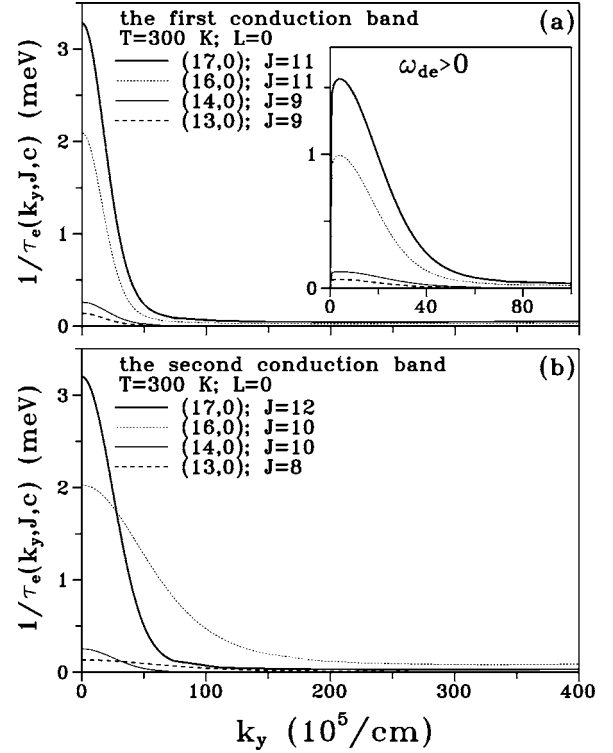


FIG. 3. The Coulomb decay rates of moderate-gap CNs for (a) the first and (b) the second conduction bands. Also shown in the inset of (a) are those associated with positive decay energies.

small  $(q, \omega_{de})$ , or the loss spectrum is sufficiently strong only in that case.  $\omega_{de}$  is much smaller than the thermal energy at  $T=300$  K; therefore,  $n_B(-\omega_{de})$  is inversely proportional to  $\omega_{de}$ . For a given  $q$ , the  $k_y=0$  state of the first band has the smaller  $n_B(-\omega_{de})$  (the larger  $\omega_{de}$ ; the smaller effective mass), compared with that of the second band. However, the former exhibits the stronger loss spectrum. The number of deexcitation channels competes with the loss spectrum so that the  $k_y=0$  decay rates of the lowest two bands are almost the same as each other [Figs. 3(a) and 3(b)].

The dependence of the Coulomb decay rate on wave vector directly reflects the feature of energy dispersion (Figs. 3 and 1). For a given  $q$ , the number of deexcitation channels  $n_B(-\omega_{de})$  declines very quickly as  $k_y$  increases. The loss spectrum might grow or decrease in the increment of  $k_y$ . Compared to the latter, the former predominates in the  $k_y$  dependence of the decay rate. As a result, the decay rate decreases with increasing  $k_y$ . The stronger the energy dispersion is, the smaller the decay rate is. The second conduction bands of the (13,0) and (16,0) CNs have the weaker  $k_y$  dependence, and so are the decay rates.

The temperature dependence of the decay rate of the band-edge state is similar for the first and the second conduction bands.  $1/\tau_e(k_y=0, J, c)$ , as shown in Fig. 4 for the first conduction band, is very sensitive to the change in temperature. The decay rate is almost vanishing for  $T < 200$  K and drastically changes near room temperature, e.g.,  $[\tau_e(T=350)]^{-1}/[\tau_e(T=300)]^{-1} > 6$ . This result means that temperature should play a very important role in experimental measurements. The temperature dependence arises from the

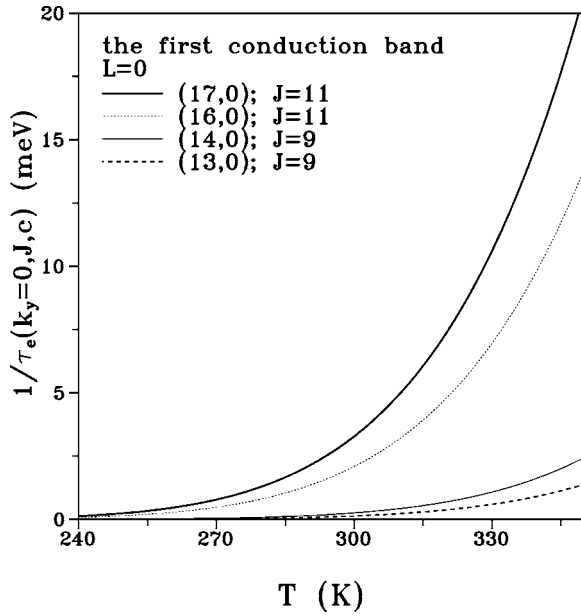


FIG. 4. The temperature-dependent decay rates for the  $k_y=0$  band-edge state of the first conduction band.

final-state distribution functions and the loss function. The second term in Eq. (3) can be approximated as  $k_B T / \omega_{de}$  for  $E^c(k_y, J) \gg k_B T$  and  $\omega_{de} \ll k_B T$ . The loss function is proportional to the imaginary part of the dielectric function [Figs. 2(a) and 2(c)], and the  $T$  dependence of  $\epsilon_2$  is mainly determined by the free carrier density with the exponential function. As a result, the decay rate of the band-edge state exhibits the complicated temperature dependence, the composite behavior of linear and exponential functions.

The above-mentioned calculations could be generalized to chiral CNs. All moderate-gap CNs exhibit similar excitations and deexcitations, the low-frequency and weak intraband  $e$ - $h$  excitations and the strong dependence of  $1/\tau_e$  on  $(k_y, T, r)$ . The decay rate of the band-edge state is strongly dependent on radius, while it is weakly affected by chirality. For example,  $1/\tau_e(k_y=0, J, c)$  of the lowest conduction band is (3.25 meV, 3.03 meV, 3.68 meV) for [(17,0), (16,3), (11,10)] CNs.

Our results roughly agree with the measured ultrafast optical spectra. Such spectra show that the fast decay time is, respectively,  $\tau \sim 0.3$ – $1.5$  ps (Refs. 11–15 and 18) and  $\tau \sim 0.13$ – $0.77$  ps (Refs. 11–13 and 15) for the first and the second conduction bands. The measured decay time is roughly consistent with the predicted result  $\tau \sim 0.5$ – $1$  ps at room temperature. The consistence clearly illustrates that the Coulomb inelastic scatterings are the important mechanism for the intraband carrier deexcitations. It should be noticed that the decay time quickly decreases as temperature increases, e.g.,  $\tau \sim 0.1$  ps for the (17,0) CN at  $T=350$  K. The temperature-dependent ultrafast optical spectra are needed for a closer study of carrier deexcitations. The carrier recombination rate due to the interband Coulomb interactions ( $c \rightarrow v$  and  $L=0$ ) is also calculated for the first conduction band.  $\tau'$  of the (17,0) CN is about 50 ns. It is much longer than the measured results (5–120 ps).<sup>13–17</sup> The interband Coulomb decay cannot account for the slow decay time. The

other scattering mechanisms need to be taken into account in the further studies, e.g., the electron-phonon interaction<sup>22</sup> and the electron-impurity scattering.

Some comments on this work and the related works are made as follows. The self-energy in Eq. (1) could be used to calculate the quasiparticle energy bands and the Coulomb lifetime. The imaginary part and the real part of the self-energy, respectively, correspond to the Coulomb decay rate and the quasiparticle energy. The former is studied in this work. The latter would affect the subband spacings, the energy gap, and the energy dispersions. These changes would be reflected in the carrier distribution function, the dielectric function, and the Coulomb deexcitations. The self-consistent calculations (recalculations of the dielectric function and the loss spectrum) are required to obtain the Coulomb decay rates of the quasiparticles. Such calculations are too massive to be done. In general, the Coulomb decay rate is directly calculated from the imaginary part of the self-energy, e.g., the previous studies on electron gases, metals, semiconductors,<sup>27–29</sup> and nanotube-related graphite systems.<sup>30</sup> In short, the quasiparticle energies would modify the electronic structure and thus the Coulomb decay rates. However, that the Coulomb decay rate strongly depends on wave vector, radius, and temperature is expected to remain unchanged.

The environments, such as the charged impurity and the background dielectric constant ( $\epsilon_0$ ),<sup>7</sup> could affect the carrier lifetime. The potential field due to the charged impurity would be screened by the  $e$ - $e$  Coulomb interactions. The scattering rate between the carrier and the charged impurity is mainly determined by the effective potential and the concentration of impurities. In addition, Perebeinos *et al.* studied the effects of  $\epsilon_0$  on excitons.<sup>24</sup> The larger the background dielectric constant is, the weaker the loss spectrum is. The Coulomb decay declines as the background dielectric constant grows.

When carbon nanotubes are excited by the EM wave, the single-particle excited states and the two-particle excitons might survive simultaneously.<sup>25,26</sup> The measured lifetimes from the femtosecond optical spectra are associated with the lifetimes of the excited carriers and excitons.<sup>11–19</sup> Spatarau *et al.* and Perebeinos *et al.*, respectively, study the excitonic effects on absorption spectra and the main features of excitons (Refs. 23 and 24). The excitonic effects would alter the two-particle wave function by mixing the states in the first and second bands. According to the mixing weights, the decay rates of the two-particle states are roughly estimated to be the linear superposition of those of the first and second bands. The dependence of the decay rate on wave vector would be changed, especially for the (16,0) and (13,0) CNs. On the other hand, the decay rate of the band-edge state almost keeps the same.

Hagen *et al.* used the time-resolved PL spectroscopy to study the decay rate of the low-concentration (6,4) CN.<sup>19</sup> The observed monoexponential dependence on time might support the notion that light emission is associated with exciton decay and not with free carrier recombination. The nonradiative decay of excitons due to charged impurities or structural defects is deduced to predominate over the PL lifetimes. As a result of the thermally activated process, the decay rate

is about a constant between 48 K and 60 K, and then grows quickly between 60 K and 182 K ( $1/\tau$  from 0.04 meV/0.2 meV; or  $\tau$  from 100 ps to 20 ps). On the other hand, this work is mainly focused on the Coulomb decay rate of the single-particle excited states. The chosen CNs are much larger than the (6,4) CN. The temperature, which causes the low-frequency excitations and deexcitations, needs to be higher than 240 K. Moreover, the predicted temperature dependence of the decay rate is much stronger than the observed result. The disagreement suggests that the Coulomb deexcitations are effective for the large CNs and the sufficiently high temperatures.

In conclusion, we have studied the temperature-induced electronic excitations and deexcitations in moderate-gap CNs. The low-frequency intraband  $e-h$  excitations, which come from some free carriers, are the effective deexcitation channels of the excited conduction electrons. The Coulomb scattering rates strongly depend on wave vector, temperature,

and radius. The band-edge state has the largest decay rate.  $1/\tau$  quickly grows in the increasing of temperature. The larger the radius is, the faster the excited conduction electrons can decay. On the other hand, the decay rate of the band-edge state is weakly affected by the chiral angle. These results arise from the strong energy dispersion and the temperature-dependent electron distribution. The calculated results roughly agree with the experimental measurements in the fast decay time. The  $e-e$  Coulomb interactions might dominate over the intraband carrier deexcitations. The further theoretical calculations are required to clarify the issue in the slow decay time; furthermore, the decay mechanisms of the two-particle excitons deserve detailed investigations. The predicted strong wave vector, temperature, and radius dependence have yet to be identified experimentally.

This work was supported by the National Science Council of Taiwan, under the Grant No. NSC 93-2112-M-006-002.

- 
- <sup>1</sup>S. Iijima, *Nature (London)* **354**, 56 (1991).  
<sup>2</sup>J. W. Mintmire, B. I. Dunlap, and C. T. White, *Phys. Rev. Lett.* **68**, 631 (1992).  
<sup>3</sup>N. Hamada, S. I. Sawada, and A. Oshiyama, *Phys. Rev. Lett.* **68**, 1579 (1992).  
<sup>4</sup>For the details of geometric and electronic structures see M. F. Lin and K. W.-K. Shung, *Phys. Rev. B* **52**, 8423 (1995).  
<sup>5</sup>J. W. G. Wilder, L. C. Venema, A. G. Rinzler, R. E. Smalley, and C. Dekker, *Nature (London)* **391**, 59 (1998).  
<sup>6</sup>T. W. Odom, J. L. Huang, P. Kim, and C. M. Lieber, *Nature (London)* **391**, 62 (1998).  
<sup>7</sup>For the details of the temperature-dependent dielectric function see M. F. Lin and F. L. Shyu, *Physica B* **292**, 117 (2000).  
<sup>8</sup>G. Gumbs, *Phys. Rev. B* **66**, 205413 (2002).  
<sup>9</sup>H. Ajiki and T. Ando, *Physica B* **201**, 349 (1994).  
<sup>10</sup>C. W. Chiu, F. L. Shyu, C. P. Chang, D. S. Chuu, and M. F. Lin, *J. Phys. Soc. Jpn.* **73**, 2936 (2004).  
<sup>11</sup>J.-S. Lauret, C. Voisin, G. Cassaboiss, C. Delalade, Ph. Rousignol, O. Jost, and L. Capes, *Phys. Rev. Lett.* **90**, 057404 (2003); *Appl. Phys. Lett.* **85**, 3572 (2004).  
<sup>12</sup>O. J. Korovyanko, C.-X. Sheng, Z. V. Vardeny, A. B. Dalton, and R. H. Baughman, *Phys. Rev. Lett.* **92**, 017403 (2004).  
<sup>13</sup>G. N. Ostojic, S. Zaric, J. Kono, M. S. Strano, V. C. Moore, R. H. Hauge, and R. E. Smalley, *Phys. Rev. Lett.* **92**, 117402 (2004).  
<sup>14</sup>L. Huang, H. N. Pedrosa, and T. D. Krauss, *Phys. Rev. Lett.* **93**, 017403 (2004).  
<sup>15</sup>M. Ichida, Y. Hamanaka, H. Kataura, Y. Achiba, and A. Nakamura, *J. Phys. Soc. Jpn.* **73**, 3479 (2004).  
<sup>16</sup>S. Reich, M. Dworak, A. Hoffmann, C. Thomsen, and M. S. Strano, *Phys. Rev. B* **71**, 033402 (2005).  
<sup>17</sup>F. Wang, G. Dukovic, L. E. Brus, and T. F. Heinz, *Phys. Rev. Lett.* **92**, 177401 (2004).  
<sup>18</sup>F. Wang, G. Dukovic, E. Knoesel, L. E. Brus, and T. F. Heinz, *Phys. Rev. B* **70**, 241403(R) (2004).  
<sup>19</sup>A. Hagen, M. Steiner, M. B. Raschke, C. Lienau, T. Hertel, H. Qian, A. J. Meixner, and A. Hartschuh, *Phys. Rev. Lett.* **95**, 197401 (2005).  
<sup>20</sup>T. Hertel and G. Moos, *Phys. Rev. Lett.* **84**, 5002 (2000).  
<sup>21</sup>M. Zamkov, N. Woody, B. Shan, Z. Chang, and P. Richard, *Phys. Rev. Lett.* **94**, 056803 (2005).  
<sup>22</sup>R. A. Jishi, M. S. Dresselhaus, and G. Dresselhaus, *Phys. Rev. B* **48**, 11385 (1993).  
<sup>23</sup>C. D. Spataru, S. Ismail-Beigi, L. X. Benedict, and S. G. Louie, *Phys. Rev. Lett.* **92**, 077402 (2004).  
<sup>24</sup>V. Perebeinos, J. Tersoff, and P. Avouris, *Phys. Rev. Lett.* **92**, 257402 (2004).  
<sup>25</sup>M. Y. Sfeir, F. Wang, L. Huang, C.-C. Chuang, J. Hone, S. P. O'Brien, T. F. Heinz, and L. E. Brus, *Science* **306**, 1540 (2004).  
<sup>26</sup>S. M. Bachilo, M. S. Strano, C. Kittrell, R. H. Hauge, R. E. Smalley, and R. B. Weisman, *Science* **298**, 2361 (2002).  
<sup>27</sup>G. D. Mahan, *Many-Particle Physics* (Plenum, New York, 1990).  
<sup>28</sup>G. F. Giuliani and J. J. Quinn, *Phys. Rev. B* **26**, 4421 (1982).  
<sup>29</sup>L. Zheng and S. Das Sarma, *Phys. Rev. B* **53**, 9964 (1996).  
<sup>30</sup>M. F. Lin and K. W.-K. Shung, *Phys. Rev. B* **53**, 1109 (1996).